Wet-Chemical Synthesis of Doped Colloidal Nanoparticles: YVO_4:Ln (Ln = Eu, Sm, Dy)

K. Riwotzki and M. Haase*

Institut für Physikalische Chemie, Universität Hamburg, Bundesstrasse 45, D- 20146 Hamburg, Germany

Received: May 19, 1998

Colloidal solutions and redispersible powders of nanocrystalline, lanthanide-doped YVO_4 have been prepared via a hydrothermal method at 200 °C. High-resolution transmission electron micrographs of size-selected samples show highly crystalline particles ranging in size from about 10 to 30 nm. The particles exhibit the tetragonal zircon structure known for bulk material. Upon UV excitation of the vanadate host, the energy is transferred to the lanthanide ion and strong luminescence (f−f transitions) is observed. By analyzing line splitting and intensity pattern in the luminescence spectrum of the europium-doped sample, we are able to verify that the dopant ions enter the same lattice site as in bulk material despite the nanocrystalline nature of the sample and the low-temperature synthesis. For YVO_4:Eu nanoparticles a luminescence quantum yield of 15% at room-temperature was observed.

Introduction

The spectroscopic properties of nanocrystalline materials are under extensive study and have been discussed in several reports and review papers. The main work during the past decade focused on semiconductor nanocrystallites since their spectroscopic data provide information on their electronic energy structure.[1]

While a wealth of journal papers exist on the preparation and the properties of undoped nanocrystallites, much fewer reports have been published on the synthesis and the properties of doped nanoparticles.

Nanocrystalline powders of Y_2SiO_5:Eu, for instance, were obtained by a sol−gel method, in which a gel prepared from $Y(NO_3)_3$, $Eu(NO_3)_3$, and $Si(OCH_3)_4$ was calcinated at 1100 °C.[2] Nanocrystalline Y_2O_3:Eu has been prepared by combustion synthesis[3] and by homogeneous precipitation of Y^{3+} and Eu^{3+} with urea followed by calcination of the precipitate at 980 °C.[4] Powders of 7−30 nm particles of the same material have been synthesized by CO_2-laser vaporization of ceramic pellets and condensing the nanocrystals from the gas phase.[5] Terbium-doped Y_2O_3 nanoparticles have been synthesized from the metal alkoxides by sol−gel processing.[6]

However, examples are rare where the properly doped nanocrystalline material is directly crystallized from an aqueous or organic solution without subsequent calcination. The advantage of this type of preparation is that well-separated nanocrystals can be obtained which in many cases can be redissolved in appropriate solvents to yield transparent and scatter-free colloidal solutions. These colloids can be investigated with the same spectroscopic techniques as used for solutions of molecules. Methods of this kind have been extensively employed for the preparation of undoped semiconductor nanocrystallites but only for a few doped II−VI nanocrystals.[7,8] The most thoroughly investigated of the latter systems is manganese-doped zinc sulfide.[7] In this case, incorporation of the manganese into the host lattice was verified by EXAFS.[7j] Furthermore, CdS, CdSe, and ZnO nanoparticles have been prepared by a solution synthesis in the presence of erbium(3+). In these cases, however, it was found that most of the erbium ions bind to the particle surface via OH bridges.[8] This shows that one has to prove that the dopant ions neither form a separate crystalline phase nor are only deposited onto the outer surface of the particles or enter the host lattice, for example, as interstitials. In a solution-phase synthesis, the latter may happen not only because the surface-to-volume ratio is much higher in the nanocrystalline systems but also because the synthesis temperature in the liquid phase is restricted to temperatures below about 400 °C, i.e., much lower than the temperatures employed in solid-state reactions. Proving that the dopant occupies a site known from the bulk material, however, requires an analytical tool that is sensitive to the local environment of the dopant ion in the nanocrystalline host. An often applied technique is EXAFS spectroscopy, which was used to investigate nanocrystalline Y_2O_3:Tb[6b] and ZnS:Mn.[7j]

In all the nanocrystalline systems mentioned above, the dopant ion acts as a luminescence center. After UV excitation of the host, energy transfer to the dopant ions occurs and the characteristic emission of the luminescence center is observed (d−d transitions in case of manganese; f−f transitions in case of Eu^{3+}, Tb^{3+}, and Er^{3+}). Deviations from the luminescence behavior of the bulk material have been reported for nanocrystalline ZnS:Mn, Y_2O_3:Tb (increased efficiencies[6,7a]), and Y_2O_3:Eu (improved concentration quenching[3]) and have been assigned to the small size of the particles. Furthermore, the properties of nanocrystalline Y_2O_3:Eu seem to depend on the preparation method: while a blue-shift in the luminescence spectrum and a decrease of the unit cell volume have been reported for a material synthesized by a sol−gel method,[4] only a weak broadening of the luminescence lines has been reported for the material prepared by CO_2-laser vaporization.[5]

In this paper, we report on the wet-chemical synthesis and characterization of lanthanide-doped YVO_4 nanoparticles. Bulk YVO_4 has been extensively used as a host for lanthanide ions[9] since high luminescence quantum yields are observed for the f−f transitions. The lanthanide ion substitutes for yttrium in the YVO_4 lattice. This site has D_{2d} symmetry, which gives rise to a characteristic crystal field splitting of the energy levels and a characteristic intensity pattern of the luminescence lines. In the case of europium, the luminescence line spectrum is relatively easy to analyze since the strongest transitions originate

10.1021/jp982293c CCC: $15.00
Published on Web 11/14/1998

from an energy state not split by the crystal field. Consequently, the Eu^{3+} ion has been extensively used to probe the local environment of dopant sites. Due to this property and because bulk YVO_4:Eu is known for its high photoluminescence quantum yield of about 70%, most of the work reported here involves doping with europium.

Bulk YVO_4:Eu also has a high luminescence efficiency upon electron-beam excitation. For this reason it had been extensively used as red phosphor in cathode ray tubes, before it was replaced by the even more efficient Y_2O_2S:Eu in the early 80s. Bulk YVO_4:Eu is usually prepared by solid-state reactions at temperatures above 1300 K,[10] but other methods including hydrothermal means have been described as well.[11] However, no report has been given on the preparation of nanocrystalline material so far.

Experimental Section

Preparation of Colloidal YVO_4:Ln. *Method a.* In a Teflon vessel 3.413 g of $Y(NO_3)_3 \cdot 6H_2O$ (8.9 mmol) and 0.209 g of $Eu(NO_3)_3 \cdot 6H_2O$ (0.47 mmol) were dissolved in 30 mL of distilled water. To the well-stirred solution, 2.730 g of $Na_3VO_4 \cdot 10H_2O$ (7.5 mmol) dissolved in 30 mL of distilled water was added. The white suspension obtained after stirring for 20 min had a pH value of about 4.8. The Teflon vessel containing the suspension was loosely capped and placed in an autoclave (Roth, 200 mL). To allow heat transfer to the vessel and avoid additional water loss of the suspension, the space between the inner wall of the autoclave and the Teflon vessel was filled with water to the same height as the suspension in the vessel. The autoclave was closed and the suspension subsequently heated to 200 °C with stirring. After 1 h the autoclave was quenched in cold water and the suspension was removed. Subsequently, the suspension was centrifuged at 3000*g* for 10 min and the supernatant was discarded. The precipitate was suspended in 40 mL of distilled water, and 3.220 g of an aqueous solution (60 wt %) of 1-hydroxyethane-1,1-diphosphonic acid (9.38 mmol) was added. To dissolve $Y(OH)_3$ formed by the excess yttrium ions under the hydrothermal treatment, the pH value of the suspension was adjusted to 0.3 with HNO_3, and the mixture was stirred for 1 h. During this treatment the color of the solution turned reddish due to the formation of colloidal V_2O_5. Subsequently, the suspension was brought to pH 12.5 with concentrated NaOH and stirred overnight in a capped vessel. The reddish colloidal V_2O_5 reacted at this pH to soluble colorless sodium vanadate, and all excess metal ions form soluble complexes with the diphosphonic acid. The latter was checked in an experiment where no vanadate at all was employed. The white suspension obtained was centrifuged at 3000*g* for 10 min, and the colorless supernatant containing the byproducts was discarded. The precipitate consists of YVO_4:Eu as determined by its X-ray powder diffraction pattern and its luminescence spectrum. The overall reaction yield is about 80−85% with respect to the amount of vanadate employed. In the next step, 40 mL of distilled water was added to the wet precipitate with stirring, resulting in peptization of the precipitate. From the resulting milky colloid containing a broad size distribution of submicrometer-sized doped YVO_4 particles, the nanoparticles were separated as described below.

Method b. A 4.095 g amount of $Y(NO_3)_3 \cdot 6H_2O$ (10.7 mmol) and 0.251 g of $Eu(NO_3)_3 \cdot 6H_2O$ (0.56 mmol) were dissolved in 15 mL of distilled water, and the solution was poured into a Teflon vessel. To the well-stirred solution, 15 mL of 1 M NaOH were added rapidly resulting in a white suspension. While the suspension was stirred, 30 mL of solution containing 2.73 g of $Na_3VO_4 \cdot 10H_2O$ (7.5 mmol) in distilled water was added dropwise. Finally the reaction mixture was adjusted to pH 12.5 with 4 M NaOH. The loosely capped Teflon vessel was placed in an autoclave and heated at 200 °C for 1 h. The suspension obtained was treated as described in method a.

Isolation of the Nanoparticles. Nanoparticles with sizes below 30 nm were isolated by employing two centrifugation steps. In the first step, the colloid was centrifuged at 3000g for 10 min. The milky supernatant obtained was decanted from the precipitate and stored. The precipitate was resuspended in 40 mL of water and centrifuged again, and the supernatant was decanted. In the second step, the combined supernatants of the first step were centrifuged at 60 000*g* for 10 min. The transparent colorless supernatant, containing the smallest nanoparticles, was carefully decanted. Finally, molecular impurities were removed by dialyzing the colloid against water (dialysis tubing: Serva, MWCO 12−14 kD). The yield of nanocrystalline YVO_4:Eu after dialysis was about 3% with respect to the total amount of vanadate employed. The colloidal solutions used in this paper had a typical concentration of 4×10^{-4} M and a pH value between 6 and 7.

Nanocrystalline Powders. Powders of the nanoparticles were obtained by removing the water of the colloidal solution with a rotary evaporator (bath temperature 50 °C). The powders obtained could be easily redispersed in water.

Characterization Techniques. Transmission electron micrographs of the particles were taken by using a CCD camera (Gatan, model no. 694) connected to a Philips CM 300 UT electron microscope, working at 300 kV acceleration voltage. A Philips X'pert system was used to measure the X-ray diffraction pattern of powder samples.

UV−vis absorption spectra of the colloidal solutions were measured with a Lambda 40 spectrometer (Perkin-Elmer). Photoluminescence spectra were recorded with a Spex Fluoromax 2 spectrometer or with a modular spectrometer with collection at 90° and resolution of 0.5 nm. The excitation module of the modular spectrometer consisted of a 450 W Xe lamp and a GCA/McPherson Instrument monochromator. The photoluminescence of the sample was detected in single-photon-counting mode by using a Spex 1672 monochromator and a Peltier-cooled photomultiplier.

Dilute colloidal solutions of YVO_4:Eu nanoparticles were placed in 1 cm cuvettes, and their absorption and luminescence were measured. The room-temperature quantum yields of the scatter-free colloidal solutions were determined by comparing the integrated emission of the colloidal solution to the emission of a solution of rhodamine 6G (Lambda Physics, laser grade; in spectroscopic grade ethanol) of identical optical density at the excitation wavelength. This method is usually employed for colloids of nanocrystals (see, for instance ref 12). The optical densities of all solutions were below 0.2 at the excitation wavelength used. No integrating sphere was used, since the radial distribution of luminescence light emitted from dilute, scatter-free solutions with similar refractive indices is independent of the emitter dissolved.

Results and Discussion

Figure 1 shows transmission electron micrographs (TEM) of the YVO_4:Eu nanoparticles prepared by methods a and b, respectively. As can be seen from the upper part of the figure, both colloids consist of particles ranging in size from about 10 to 30 nm. The morphology of the particles is slightly different for the two preparation methods: particles prepared in strongly

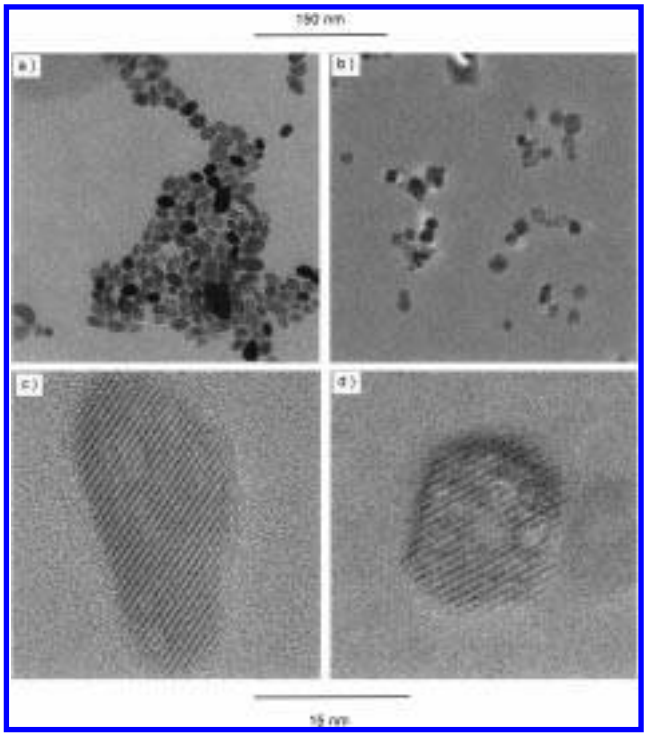

Figure 1. Top part: TEM micrographs of ensembles of YVO_4:Eu nanoparticles prepared by methods a (left) and b (right), respectively. Bottom part: High-resolution TEM micrographs showing lattice fringes of single YVO_4:Eu nanoparticles prepared by methods a (left) and b (right), respectively.

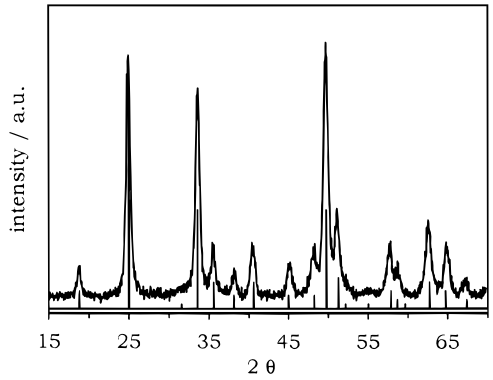

Figure 2. XRD pattern of nanocrystalline YVO_4:Eu powder. The line spectrum corresponds to literature data given for wakefieldite (PDF No. 17-341).

alkaline solution (method b) show better defined crystal facets and edges than those prepared under acidic conditions. High-resolution TEM images of both colloids are shown in the lower part of the figure. The particles in the figure show well defined (200) lattice fringes with 3.6 Å spacing, providing proof that both preparation methods yield particles of high crystallinity.

The crystal phase of the nanoparticles was determined by X-ray powder diffraction (Figure 2). The XRD pattern of the nanocrystalline powder is identical for both preparation methods and is completely consistent with the tetragonal zircon structure known from bulk YVO_4. The mean particle size can be roughly determined from the broadening of the peaks by using the Scherrer formula. By fitting various peaks to this formula and taking into account the instrumental broadening, we obtained values between 15 and 18 nm for the particle diameter, in accord with the particle size observed in the TEM pictures.

The optical and spectroscopic properties of the nanoparticles are found to be independent of the preparation method. Neither

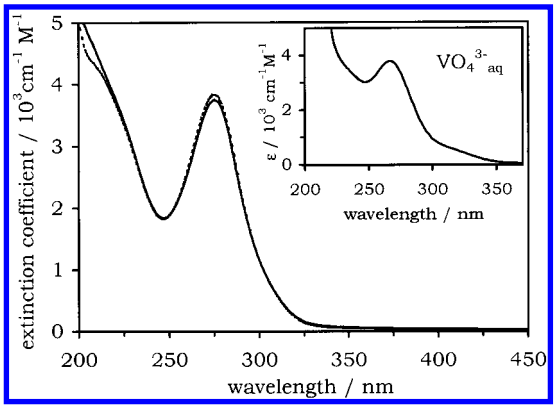

Figure 3. UV−vis absorption spectra of a 4×10^{-4} M colloidal solution of nanocrystalline YVO_4:Eu: broken line, colloid after preparation; solid line, colloid obtained by redispersing dry nanocrystalline powder in water. Inset: UV−vis absorption spectrum of the VO_4^{3-} ion (i.e. aqueous solution of Na_3VO_4 at pH 13).

in the UV−vis absorption nor in the emission and excitation spectra could differences between the two preparation methods be detected. The results presented in the following figures, therefore, apply to both preparation methods.

Figure 3 shows the UV−vis absorption spectrum of a 4×10^{-4} M aqueous colloid. A strong absorption is observed in the UV region with a maximum at 272 nm (broken line). To prove the redispersibility of the nanoparticles, we removed all water from the colloidal solution with a rotary evaporator and, subsequently, redispersed the dry powder in the same amount of water. After the sample was stirred for 2−3 min, a transparent colloid was obtained displaying the absorption spectrum shown as solid line in Figure 3. Obviously, the resulting absorption displays the same intensity and shape as before. No contribution of light scattering is observed in the spectrum indicating that the nanoparticles did redissolve completely. The extinction coefficients given in the figure were determined by redispersing a weighted amount of the nanocrystalline powder and measuring the absorbance of the resulting transparent colloid. For nanocrystalline $Y_{0.95}Eu_{0.05}VO_4$ (M_w = 0.207 kg mol^{-1}), we obtain an extinction coefficient of ϵ(272 nm) $\approx 4 \times 10^3$ dm^3 mol^{-1} cm^{-1} at the absorption maximum.

The interaction of the VO_4^{3-} groups in bulk YVO_4 is known to be comparatively weak.[13] The first excited state has mainly the character of a localized charge-transfer state where electron density shifts from the oxygen ligands to the central vanadium atom. In fact, the UV−vis absorption of an aqueous solution of the VO_4^{3-} ion (i.e. a basic aqueous solution of Na_3VO_4, as shown in the inset of Figure 3) exhibits an oscillator strength and a spectral position ($\epsilon_{max} = 3.8 \times 10^3$ dm^3 mol^{-1} cm^{-1} at $\lambda_{max} = 267$ nm) similar to the first transition of the YVO_4 colloid. If we, therefore, roughly assume that the first optical transition is only weakly affected by the nature of the embedding medium and the nanocrystalline size of the particles, we may calculate the absorption coefficient of a compact layer of YVO_4 from the extinction coefficient by

$$\alpha = \epsilon \frac{\rho \ln 10}{M_w}$$

Using $\rho = 4.2$ kg dm^{-3} for the density of YVO_4 and M_w = 0.203 kg mol^{-1} for its molecular weight, we obtain an absorption coefficient of $\alpha_{max} = 2 \times 10^5$ cm^{-1} at 272 nm.

Figure 4 shows a part of the energy level diagram of the Eu^{3+} ion in a solid host. The $^7F_0$ level is the highest level occupied (at 0 K). Many more levels are known at energies higher than

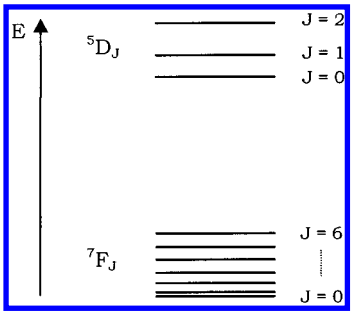

Figure 4. Part of the energy level diagram of the Eu^{3+} ion. Only energy levels are given which are involved in transitions observed in the luminescence spectrum.

the $^5D_2$ level.[14] While the overall energy level structure of the Eu^{3+} ion does not change in different hosts due to the shielding of the 4f electrons by outer shell 5s and 6p electrons, each energy level shown in the figure can be split into up to $2J + 1$ sublevels by the local crystal field surrounding the Eu^{3+} ion. In fact, the lines observed in the luminescence spectrum correspond to transitions between sublevels of the energy levels shown in the figure.

The intensity of transitions between different *J*-number levels depends on the symmetry of the local environment of the europium ion and can be described in terms of the Judd−Ofelt theory.[15] In bulk YVO_4 the Eu^{3+} ion occupies a site with no inversion symmetry. In this case, the selection rule for electrical dipole transitions between the levels of Figure 4 is $|\Delta J| \leq 6$ if neither the initial nor the final state has $J = 0$. In case of the latter condition, transitions are allowed only if $|\Delta J| = 2$, 4, or 6. Judd−Ofelt theory states further that magnetic dipole transitions are allowed if $|\Delta J| = 0$ or 1 (but not $J = 0 \rightarrow J' = 0$), regardless of environment. For lanthanides the spin−orbit coupling is intermediate between Russel−Saunders coupling and *j*−*j* coupling.[15c] Therefore, only *J* is considered a good quantum number. Nevertheless, ^{2S+1}L labels are often used even for the higher excited states of the lanthanides.

To analyze the transitions observed in the luminescence spectrum, the crystal field splitting of the energy levels has also to be taken into account. In bulk YVO_4 the Eu^{3+} site has D_{2d} symmetry. For this point group, the splitting of the energy levels has been calculated and the selection rules for transitions between the sublevels are well-known. They are in good agreement with the optical transitions actually observed in bulk YVO_4:Eu.[16]

By varying the europium content of the nanocrystals, we determined the composition with the highest luminescence intensity (Figure 5). Similar to bulk material[9] the quantum yield shows a maximum at a doping level of about 5 mol % europium and slowly decreases at higher europium concentrations. This partial quenching of the luminescence at high europium concentrations is a typical property of lanthanide-doped systems and is observed if the mean distance between neighboring europium ions decreases below a critical value. The underlying mechanisms of this "concentration quenching" are well investigated for various bulk systems (for details, see ref 17). The typical nonlinear variation of the quantum yield shown in Figure 5 is important, because it provides additional proof that the sample consists of doped particles and not of a mixture of $EuVO_4$ and YVO_4 particles. In the latter case the quantum yield is expected to steadily increase with increasing europium content.

Since temperature-dependent luminescence lifetime measurements are beyond the scope of this paper, information on the

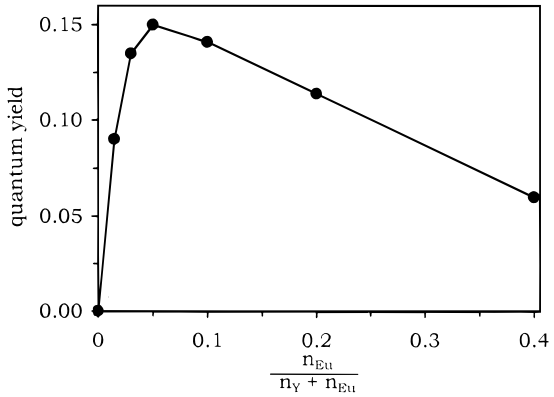

Figure 5. Luminescence quantum yield as a function of the Eu^{3+} concentration in the YVO_4 nanocrystals.

mechanism of the concentration quenching and the energy migration inside the nanoparticles are not yet available.

The luminescence spectrum of our colloidal solution is shown in the Figures 6−8. As the highest quantum yield is observed at a doping level of about 5 mol % europium, nanocrystals with the composition $Y_{0.95}Eu_{0.05}VO_4$ have been used throughout the present paper. The spectral positions of electric dipole allowed transitions predicted by the theory (given in ref 16) are indicated in the figures by vertical lines. Most of the fluorescence lines observed in bulk YVO_4:Eu can be assigned to these transitions. Longer lines indicate those transitions in each group which are reported to have the highest luminescence intensity in bulk YVO_4:Eu. Luminescence peaks marked with an asterisk have been observed also in bulk material but could not be assigned to transitions between energy levels given in Figure 4. No attempt was made to ascribe these lines to phonon side bands or to lanthanide impurities. Broken lines in Figures 7 and 8 indicate magnetic dipole allowed transitions. For clarity, we did not include magnetic dipole allowed transitions originating from the $^5D_2$ level, since they have rather low intensity in the bulk material.

The most intense transitions observed in the luminescence spectrum (Figure 6) originate from the $^5D_0$ level, which is not split by the crystal field ($J = 0$). From this level there are an electric dipole allowed transition to a sublevel of $^7F_1$, two electric dipole transitions to sublevels of $^7F_2$, three transitions to sublevels of $^7F_3$, three transitions to sublevels of $^7F_4$, and five transitions to $^7F_6$.[16] In accordance with Judd−Ofelt theory, transitions to even *J*-numbers have much higher intensity than those to corresponding neighboring odd *J*-numbers. The most intense luminescence lines correspond to the $^5D_0$−$^7F_2$ transition. As reported for bulk YVO_4:Eu, three transitions to the sublevels of $^7F_6$ appear as very weak lines in the spectrum (lower part of the figure). The intensity pattern of the transitions to the $^7F_5$ levels for bulk material has not been given. In fact, the corresponding weak lines at about 750 nm are barely detectable also in the spectrum of the nanoparticles.

In Figure 7, the luminescence spectrum of the colloidal solution is reproduced on an enlarged scale. A large number of additional transitions with lower intensity are observed, most of which can be assigned to transitions originating from the $^5D_1$ level. In YVO_4 this level is split by the crystal field into two sublevels. Within the resolution of our room-temperature spectrum, satisfactory agreement with the theoretical lines is observed. Again, the asterisk in Figure 7 marks a peak which is also observed for the bulk material but could not be assigned to transitions from either of the $^5D_0$, $^5D_1$, or $^5D_2$ levels.

If the luminescence pattern is further enlarged (Figure 8), transitions of very low intensity mainly originating from the

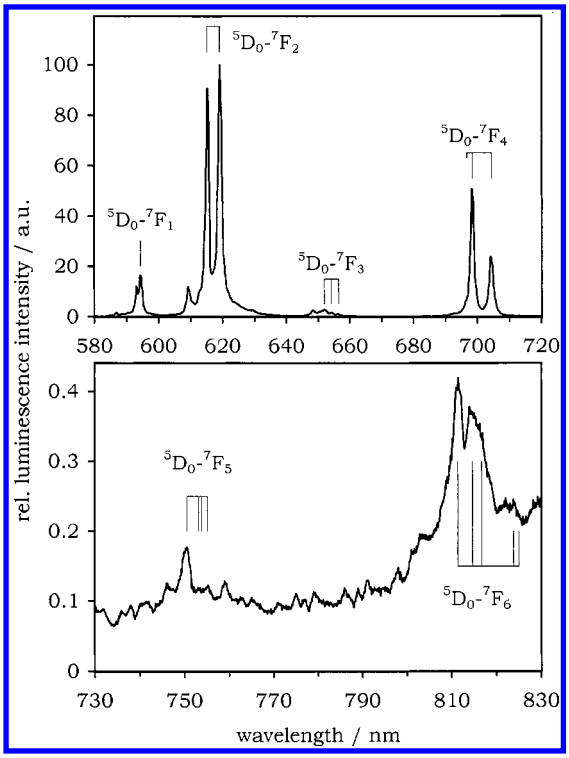

Figure 6. Luminescence spectrum of a 4×10^{-4} M colloidal solution of nanocrystalline YVO_4:Eu ($\lambda_{ex} = 310$ nm) (see text also): top part, main lines of the emission spectrum due to transitions from the $^5D_0$ level; bottom part, weak lines in the NIR region due to transitions from the $^5D_0$ level.

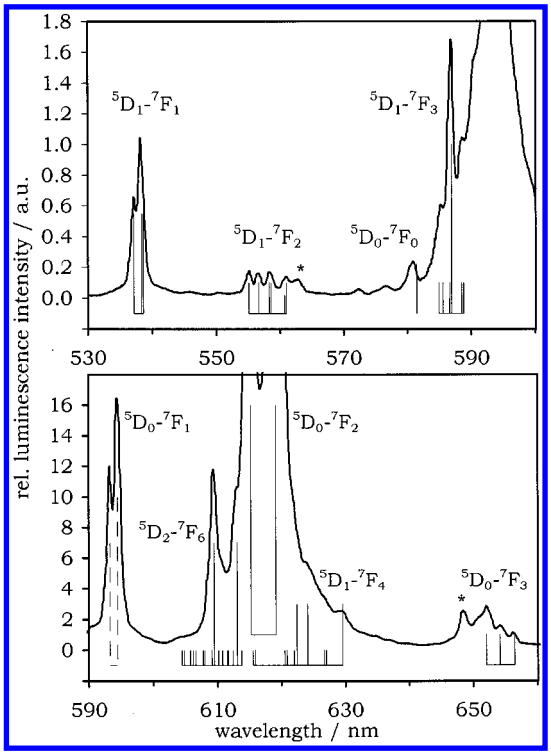

Figure 7. Enlarged portions of the luminescence spectrum showing transitions from the $^5D_1$ level in more detail.

$^5D_2$ level (split into 4 sublevels) are detected. Again, satisfactory agreement with the theoretical line positions is observed. This holds true even for the $^5D_2-{}^7F_4$ transitions for which no experimental results have been given in case of bulk YVO_4:Eu.

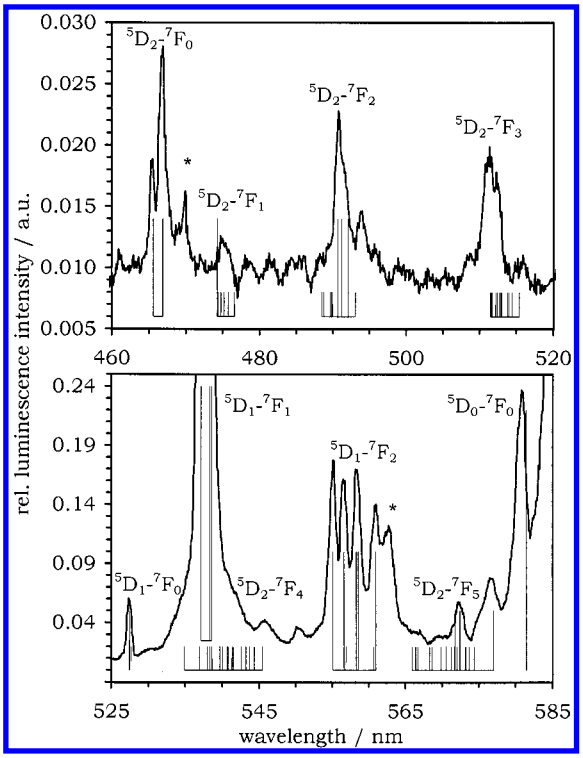

Figure 8. Enlarged portions of the luminescence spectrum showing transitions from the $^5D_2$ level in more detail.

Only two minor deviations from the spectrum reported for the bulk material are observed for the nanoparticles. First, although the group of $^5D_2-{}^7F_1$ transitions are detected at the expected positions, their reported intensity pattern deviates from the pattern observed for the nanocrystalline sample. Since we cannot resolve this group into single lines, we cannot give yet an explanation for this deviation. Second, we observe a luminescence line at 581 nm similar to a peak that is only observed in powders of bulk material but not in bulk single crystals.[16] While no explanation has been given for its absence in the case of single crystals, the peak has been assigned to the strongly forbidden $^5D_0-{}^7F_0$ transition which is expected to occur at this wavelength. The peak in our luminescence spectrum, however, is more than one nanometer off this position. Since all other transitions to the $^7F_0$ level as well as those from the $^5D_0$ level are observed at the correct positions, we cannot assign this peak to the $^5D_0-{}^7F_0$ transition. One may ask whether the unknown peak belongs to europium(3+) in an environment with different symmetry. In this case, however, the unknown peak has to be the most intense transition in this site symmetry, because other peaks not observed in bulk YVO_4:Eu are absent in our spectrum. Although either the hypersensitive $^5D_0-{}^7F_2$ transition (e.g. Eu^{3+} in Y_2O_3) or the magnetic-dipole allowed $^5D_0-{}^7F_1$ transition (Eu^{3+} site with inversion symmetry) can be the dominant transition of Eu^{3+} in an appropriate host, no site symmetry is known where the $^5D_0-{}^7F_0$ transition has the highest intensity in the spectrum. Therefore, it is unlikely that the line is caused by Eu^{3+} in a different site. A more likely explanation is that the line is caused by an impurity.

Except for these two deviations, the room-temperature luminescence spectrum of the nanoparticles agrees very well with the predicted spectrum for an Eu^{3+} ion in a D_{2d} environment. Moreover, the intensity pattern and the spectral position of the luminescence lines are in accordance with those observed for bulk YVO_4:Eu. Thus, despite the low temperature at which the nanoparticles have been synthesized, the Eu^{3+} ions have entered the YVO_4 lattice in the same site as in bulk material.

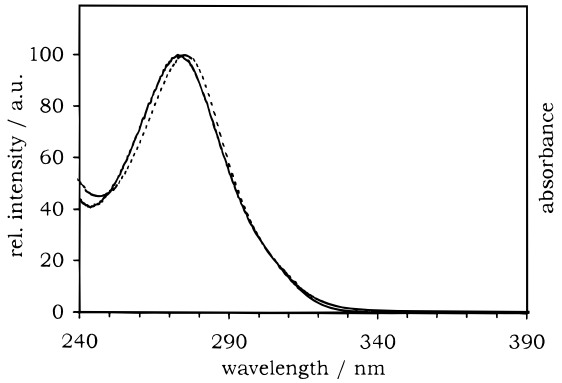

Figure 9. Solid line: Luminescence excitation spectrum of a diluted (7×10^{-5} M) colloidal solution of nanocrystalline YVO_4:Eu (λ_{em} = 618 nm). Broken line: UV−vis absorption spectrum of the same colloid at a concentration of 4×10^{-4} M.

We carefully determined the quantum yield of the YVO_4:Eu luminescence in colloidal solution at room temperature and obtained a value of 15%, which is about one-fifth of the value of bulk material. The deviation from the bulk value indicates that excitation energy is transported to centers where radiationless recombination occurs. Bulk YVO_4:Eu shows considerable energy transfer[18] via the vanadate groups as well as via adjacent europium ions at room temperature. The exciton diffusion length in bulk YVO_4:Eu has been determined to be 13 nm.[18] Hence, energy migration to the particle surface should always be possible in our nanoparticles.

Strong quenching of the europium luminescence is known to take place in metal−organic europium complexes if water molecules are bound to the central europium atom.[19] It is very feasible that water atoms or hydroxyl groups would bind to europium atoms located at the surface of the nanoparticles in an aqueous colloidal solution. Consequently, in our colloids of YVO_4:Eu nanoparticles a reduced quantum yield may be expected.

Figure 9 displays the luminescence excitation spectrum of a strongly diluted (7×10^{-5} M) $Y_{0.95}Eu_{0.05}VO_4$ colloid. The spectrum exhibits a peak-shape behavior in the UV practically identical to that for the absorption spectrum of the colloid (broken line; see Figure 3 also). The appearance of the vanadate band in the excitation spectrum shows that, after optical excitation of the host, energy transfer to the Eu^{3+} ions occurs as is the case in bulk material.[18] Note that, for a colloidal solution of YVO_4:Eu nanoparticles, the UV excitation spectrum can be easily measured despite the very high absorption coefficient of the vanadate host.

The luminescence excitation spectrum of a more concentrated colloid (1×10^{-3} M) is shown in Figure 10. The spectrum is characterized by sharp lines corresponding to direct excitation of the Eu^{3+} ground state into higher levels of the 4f manifold. In the lower part of the figure, transitions involving energy levels shown in Figure 4 are displayed in greater detail. Luminescence lines observed at wavelengths above 450 nm can all be assigned to transitions from both the $^7F_0$ level and the thermally populated $^7F_1$ levels to the ^5D levels. For comparison, the theoretically expected spectral positions of these transitions are given as vertical lines. As was the case for the emission spectra, the spectral position and the intensity of the transitions are identical to those observed for the bulk material.[16] The latter also applies to the intense lines below 450 nm corresponding to excitations into higher energy levels than the $^5D_2$ level. To describe these transitions we used ^{2S+1}L labels given in the literature.[20] At wavelengths below 350 nm the excitation spectrum shows a steep rise due to the onset of the vanadate band shown in Figure 9. Within the sensitivity of our spectrometer the strongly forbidden $^7F_0-^5D_0$ transition could not be detected.

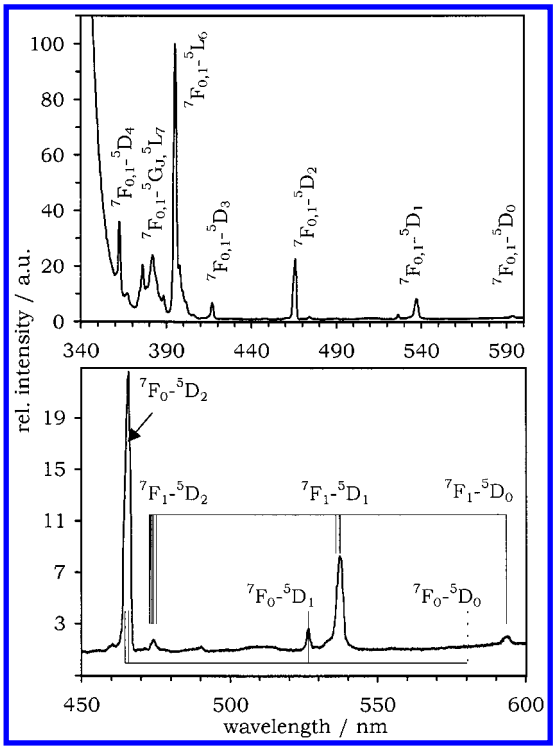

Figure 10. Luminescence excitation spectrum (λ_{em} = 618 nm) recorded at a higher concentration (1×10^{-3} M) of the YVO_4:Eu colloid: top part, line spectrum due to direct excitation of the f−f transitions; bottom part, assignment of transitions also observed in the emission spectrum.

The synthesis described above may as well be used for preparing YVO_4 doped with lanthanide ions other than europium. We show the luminescence spectra of colloidal solutions of dysprosium-doped and samarium-doped nanocrystalline YVO_4 in Figure 11. Doping levels of 2 mol % in the case of samarium and 1 mol % in the case of dysprosium have been employed, respectively. All colloids have been prepared by method b. The TEM micrographs, XRD pattern, and absorption spectra of these systems are practically identical to those of the europium-doped sample. Furthermore, the luminescence excitation spectra of the diluted colloids are identical to the spectrum shown in Figure 9. This shows that transfer of the excitation energy to the dopant ions also occurs in these materials. The luminescence line spectra of both systems are identical to those of the corresponding bulk material.[9] The main luminescence lines in each emission spectrum can be assigned to known transitions of the respective ion (Figure 11). As in bulk material, the luminescence quantum yields of both are lower than for the europium-doped samples.

Conclusion

We prepared colloids and redispersible powders of lanthanide-doped YVO_4 nanoparticles at low temperatures. The highly crystalline nanoparticles have a size of about 10−30 nm and exhibit the same tetragonal zircon structure as bulk YVO_4. Upon UV excitation of the host, energy transfer to the lanthanide ions occurs and the characteristic luminescence of their f−f transitions is observed. The luminescence spectrum of nanocrystalline YVO_4:Eu was analyzed in some detail. With two small exceptions the intensity pattern of the luminescence line spectrum is the same as observed for bulk material and the

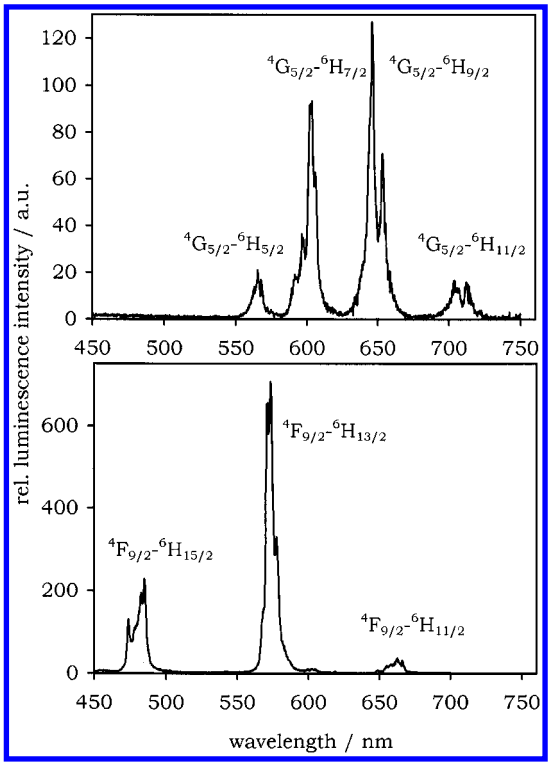

Figure 11. Solution spectra of nanocrystalline YVO_4 doped with samarium and dysprosium, respectively: top part, luminescence of Sm^{3+} after excitation of the vanadate host (λ_{ex} = 310 nm); bottom part, luminescence of Dy^{3+} after excitation of the vanadate host (λ_{ex} = 310 nm).

spectral position of the luminescence transitions correspond to those expected for an Eu^{3+} ion occupying a site with D_{2d} symmetry. Hence, despite the low-temperature synthesis at 200 °C, the dopant ion occupies the same site as in the bulk material.

Of all systems investigated, YVO_4 nanoparticles doped with europium show the strongest luminescence. For nanoparticles of the composition $Y_{0.95}Eu_{0.05}VO_4$, we determined a luminescence quantum yield of 15% at room temperature, which is about five times lower than the quantum yield of the corresponding bulk material. Doping of YVO_4 nanoparticles was also achieved with dysprosium and samarium as evidenced by their luminescence spectra.

Since the literature value of the exciton diffusion length in bulk material is similar to the size of our nanoparticles, energy migration to surface states may be an important factor determining the quantum yield. Therefore, the influence of surface coatings on the quantum yield and the luminescence lifetime will be investigated in a forthcoming paper.

Acknowledgment. We thank J. Ludwig and Dr. Klaska from the Mineralogisch-Petrographisches Institut of the University of Hamburg for the measurement of the XRD spectra and A. Kornowski and S. Naused for preparing the electron micrographs. We greatly acknowledge funding of this project by the German Science Foundation (DFG).

References and Notes

(1) (a) Henglein, A. *Top. Curr. Chem.* **1988**, *143*, 113. (b) Henglein, A. *Chem. Rev.* **1989**, *89*, 1861. (c) Brus, L. E. *Appl. Phys. A* **1991**, *53*, 465. (d) Wang, Y.; Herron, N. *J. Phys. Chem.* **1991**, *95*, 525. (e) Weller, H. *Angew. Chem., Int. Ed. Engl.* **1993**, *32*, 41. (f) Weller, H. *Adv. Mater.* **1993**, *5* (2), 88. (g) Weller, H., Eychmüller, A. In *Advance in Photochemistry*; Neckers, D. C., Volman, D. H., Bünau, G. v., Eds.; John Wiley & Sons: New York, 1995; Vol. 20, p 165. (h) Alivisatos, A. P. *J. Phys. Chem.* **1996**, *100*, 13226. (i) Alivisatos, A. P. *Science* **1996**, *271*, 933.

(2) Yin, M.; Zhang, W.; Xia, S.; Krupa, J.-C. *J. Lumin.* **1996**, *68*, 335.

(3) Ye, T.; Zhao, G. W.; Zhang, W. P.; Xia, S. D. *Mater. Res. Bull.* **1997**, *32*, 501.

(4) Li, Q.; Gao, L.; Yan, D. *Nanostruct. Mater.* **1997**, *8*, 825.

(5) (a) Williams, D. K.; Bihari, B.; Tissue, B. M.; McHale, J. M. *J. Phys. Chem. B.* **1998**, *102*, 916. (b) Bihari, B.; Eilers, H.; Tissue, B. M. *J. Lumin.* **1997**, *72*−*74*, 190.

(6) (a) Goldburt, E. T.; Kurkarni, B.; Bhargava, R. N.; Taylor, J.; Liberia, M. *J. Lumin.* **1997**, *75*, 1. (b) Soo, Y. L.; Huang, S. W.; Ming, Z. H.; Kao, Y. H.; Smith, G. C.; Goldburt, E.; Hodel, R.; Kulkarni, B.; Veliadis, J. V. D.; Bhargava, R. N. *J. Appl. Phys.* **1998**, *83*, 5404.

(7) (a) Bhargava, R. N. *J. Lumin.* **1996**, *70* (1−6), 85. (b) Hua, Yang; Zichen, Wang; Lizhu, Song; Muyu, Zhao; Yimin, Chen; Kai, Dou; Jiaqi, Yu; Li, Wang *Mater. Chem. Phys.* **1997**, *47* (2−3), 249. (c) Kobayashi, M.; Iwata, H.; Hanzawa, H.; Yoshiue, T.; Endo, S. *Phys. Stat. Sol. B (Germany)* **1996**, *198* (1), 515. (d) Bhargava, R. N.; Gallagher, D.; Sosnowski, T.; Klein, P. B.; Norris, T. B.; Soo, Y. L.; Kao, Y. H.; Kennedy, T. A.; Glaser, E. R. *22nd Int. Conf. Phys. Semicond.* **1995**, *3*, 2007. (e) Yu, Il; Isobe, T.; Senna, M. *J. Phys. Chem. Sol.* **1996**, *57* (4), 373. (f) Kennedy, T. A.; Glaser, E. R.; Klein, P. B.; Bhargava, R. N. *Mater. Sci. Forum (Switzerland)* **1995**, *196*−*201* (2), 737. (g) Kennedy, T. A.; Glaser, E. R.; Klein, P. B.; Bhargava, R. N. *Phys. Rev. B: Condens. Matter* **1995**, *52* (20), R14356. (h) Khosravi, A. A.; Kundu, M.; Kuruvilla, B. A.; Shekhawat, G. S.; Gupta, R. P.; Sharma, A. K.; Vyas, P. D.; Kulkarni, S. K. *Appl. Phys. Lett.* **1995**, *67* (17), 2506. (i) Gallagher, D.; Heady, W. E.; Racz, J. M.; Bhargava, R. N. *J. Mater. Res.* **1995**, *10* (4), 870. (j) Soo, Y. L.; Ming, Z. H.; Huang, S. W.; Kao, Y. H.; Bhargava, R. N.; Gallagher, D. *Phys. Rev. B: Condens. Matter* **1994**, *50* (11), 7602.

(8) Schmidt, T.; Müller, G.; Spanhel, L.; Kerkel, K.; Forchel, A. *Chem. Mater.* **1998**, *10*, 65.

(9) Palilla, F. C.; Levine, A. K.; Rinkevics, M. *J. Electrochem. Soc.* **1965**, *112* (8), 776.

(10) (a) Wanmaker, W. L.; Bril, A.; ter Vrugt, J. W.; Broos, J. *Philips Res. Rep.* **1966**, *21*, 270. (b) Schwarz, H. *Z. Anorg. Allg. Chem.* **1963**, *323*, 44. (c) Palilla, F. C.; Levine, A. K.; Rinkevics, M. *J. Electrochem. Soc.* **1965**, *112* (8), 776.

(11) (a) For general techniques of hydrothermal synthesis, see, for instance: Laudise, R. A. In *The Growth of Single Crystals*; Holonyak, Nick, Jr., Ed.; Solid State Physical Electronics Series; Prentice Hall International, Inc.: London, 1970; Chapter 7.3. (b) Nakhodnova, A. P.; Zaslavskaya, L. V. *Russ. J. Inorg. Chem.* **1984**, *29* (6), 835. (c) Nakhodnova, A. P.; Zaslavskaya, L. V.; Pitsyuga, V. G. *Russ. J. Inorg. Chem.* **1983**, *28* (3), 358. (d) Nakhodnova, A. P.; Zaslavskaya, L. V.; *Russ. J. Inorg. Chem.* **1982**, *27* (3), 378. (e) Ropp, R. C.; Carroll, B. *J. Inorg. Nucl. Chem.* **1977**, *39*, 1303.

(12) (a) Hines, M. A.; Guyot-Sionnest, P. *J. Phys. Chem.* **1996**, *100*, 468. (b) Peng, X.; Schlamp, M. C.; Kadavanich, A. V.; Alivisatos, A. P. *J. Am. Chem. Soc.* **1997**, *119*, 7019. (c) Dabbousi, B. O.; Rodriguez-Viejo, J.; Miculec, F. V.; Heine, J. R.; Mattoussi, H.; Ober, R.; Jensen, K. F.; Bawendi, M. G. *J. Phys. Chem. B* **1997**, *101*, 9463.

(13) (a) Blasse, G. *Philips Res. Rep.* **1968**, *23*, 344. (b) Blasse, G. *Philips Res. Rep.* **1969**, *24*, 131. (c) Blasse, G.; Bril, A. *Philips Technol. Rev.* **1970**, *31*, 304. (d) Blasse, G. *Struct. Bonding* **1980**, *42*, 1.

(14) (a) Dieke, G. H. *Spectra and Energy Levels of Rare Earth Ions in Crystals*; Interscience: New York, 1968. (b) Carnall, W. T.; Goodman, G. L.; Rajnak, K.; Rana, R. S. *J. Chem. Phys.* **1989**, *90*, 343.

(15) (a) Judd, B. R. *Phys. Rev.* **1962**, *127*, 750. (b) Ofelt, G. S. *J. Chem. Phys.* **1962**, *37*, 511. (c) Peacock, R. D. *Struct. Bonding* **1975**, *22*, 83.

(16) Brecher, C.; Samelson, H.; Lempicki, A.; Riley, R.; Peters, T. *Phys. Rev.* **1967**, *155*, 178.

(17) Blasse, G. *Prog. Solid State Chem.* **1988**, *18*, 79.

(18) (a) Hsu, Ch.; Powell, C. *J. Lumin.* **1975**, *10*, 273. (b) Blasse, G. *Energy Transfer Processes in Condensed Matter*; Plenum Press: New York, 1984.

(19) (a) Harrocks, W. DeW.; Schmidt, G. R., Jr.; Sudnick, D. R.; Kittrel, C.; Bernheim, R. A. *J. Am. Chem. Soc.* **1977**, *99*, 2378. (b) Harrocks, W. DeW. Sudnick, D. R., Jr.; *Science* **1979**, *206*, 1194. (c) Harrocks, W. DeW.; Sudnick, D. R., Jr. *Acc. Chem. Res.* **1981**, *14*, 384. (d) Hole, R. C.; Harrocks, W. DeW., Jr. *Inorg. Chim. Acta* **1990**, *171*, 193. (e) Frey, S. T.; Chang, C. A.; Pounds, K. L.; Harrocks, W. DeW, Jr. *Inorg. Chem.* **1994**, *33*, 2882.

(20) Dejneka, M.; Snitzer, E.; Riman, R. E. *J. Lumin.* **1995**, *65*, 227.